European Journal of
Mineralogy
Open Access

Ferri-taramite, a new member of the amphibole supergroup, from the Jakobsberg Mn–Fe deposit, Värmland, Sweden

Dan Holtstam[1], **Fernando Cámara**[2], **Andreas Karlsson**[1], **Henrik Skogby**[1], **and Thomas Zack**[3]

[1]Department of Geosciences, Swedish Museum of Natural History,
P.O. Box 50007, 10405 Stockholm, Sweden
[2]Dipartimento di Scienze della Terra "A. Desio", Università degli Studi di Milano,
Via Luigi Mangiagalli 34, 20133, Milan, Italy
[3]Department of Earth Sciences, University of Gothenburg, P.O. Box 460, 40530 Gothenburg, Sweden

Correspondence: Dan Holtstam (dan.holtstam@nrm.se)

Abstract. Ferri-taramite (IMA CNMNC 2021-046), ideally $^A\text{Na}\,^B(\text{CaNa})\,^C(\text{Mg}_3\text{Fe}_2^{3+})(\text{Si}_6\text{Al}_2)\text{O}_{22}\,^W(\text{OH})_2$, occurs in skarn from the Jakobsberg manganese mine, Värmland, Sweden. Associated minerals are celsian, phlogopite, aegirine-augite, andradite, hancockite, melanotekite, microcline (var. hyalophane), calcite, baryte, prehnite, macedonite and oxyplumboroméite. Conditions of formation, close to peak metamorphism (at circa 650 °C and 0.4 GPa), include silica undersaturation, a slightly peralkaline character and relatively high oxygen fugacities. Ferri-taramite forms poikiloblastic crystals up to 5 mm and is dark brownish black with a yellowish grey streak. The amphibole is brittle with an uneven to splintery fracture. Cleavage parallel to {110} is good. Hardness (Mohs) is ~ 6, and $D_{\text{calc}} = 3.227(5)\,\text{g cm}^{-3}$. Holotype ferri-taramite has the experimental unit formula $^A(\text{Na}_{0.79}\text{K}_{0.16}\text{Pb}_{0.01})_{\Sigma 0.96}\,^B(\text{Ca}_{1.26}\text{Na}_{0.72}\text{Mn}^{2+}_{0.02})_{\Sigma 2}\,^C(\text{Mg}_{2.66}\text{Mn}^{2+}_{0.58}\text{Fe}^{2+}_{0.16}\text{Zn}_{0.02}\text{Fe}^{3+}_{1.26}\text{Al}_{0.26}\text{Ti}_{0.06})_{\Sigma 5.00}\,^T(\text{Al}_{1.86}\text{Si}_{6.14})_{\Sigma 8}\text{O}_{22}\,^W(\text{OH})_2$, based on chemical analyses (EDS, laser-ablation ICP-MS) and spectroscopic (Mössbauer, infrared) and single-crystal X-ray diffraction data. The mineral is optically biaxial (–), with $\alpha = 1.670(5)$, $\beta = 1.680(5)$ and $\gamma = 1.685(5)$ in white light and $2V_{\text{meas}} = 70(10)°$ and $2V_{\text{calc}} = 70.2°$. Ferri-taramite is distinctly pleochroic in transmitted light, with X pale yellow, Y dark brown, Z yellowish brown and absorption $Y > Z > X$. The eight strongest reflections in the X-ray powder pattern (d values (in Å), I_{rel}, hkl) are 8.44, 60, 110; 3.392, 25, 131; 3.281, 39, 240; 3.140, 100, 310; 2.816, 45, 330; 2.7104, 38, 151; 1.3654, 26, 461; and 1.4451, 33, $\bar{6}61$. Refined unit-cell parameters from single-crystal diffraction data are $a = 9.89596(13)$, $b = 18.015(2)$, $c = 5.32164(7)$ Å, $\beta = 105.003(13)°$ and $V = 916.38(2)$ Å^3 for $Z = 2$. Refinement of the crystal structure yielded $R = 2.26\%$ for 2722 reflections with $I_o > 2\sigma(I)$. The Mn^{2+} and Fe^{2+} ions show preference for the $M1$ and $M3$ octahedrally coordinated sites, whereas Fe^{3+} is strongly ordered at $M2$. The A-group cations, K and Na, are split over two subsites, $A(m)$ and $A(2)$, respectively.

1 Introduction

Members of the sodium–calcium subgroup of the amphibole supergroup (general formula $AB_2C_5T_8O_{22}W_2$) associated with the root name taramite (Na(NaCa)Mg$_3$Al$_2$(Si$_6$Al$_2$)(OH)$_2$) are relatively rare. They typically occur in alkaline igneous rocks and gneisses (e.g. Giret et al., 1980), retrogressed eclogites (Zhang and Liou, 1994), and some felsic lithologies that have experi-

enced ultrahigh-pressure metamorphism (Compagnoni and Rolfo, 1999).

Ferrous compositions are the most frequent. The original "taramite", reported from a nepheline syenite in the Vali Tarama ravine, near Mariupol, Ukraine (Morozewicz, 1925), essentially represents a ferro-ferri-taramite in composition, following the current amphibole supergroup classification (Hawthorne et al., 2012). The "ferri-taramite" from Bancroft, Ontario, Canada, investigated by Hawthorne and

Grundy (1978) is also a ferro-ferri-taramite. Other specimens of ferro-taramite and ferro-ferri-taramite have been described in metabasites from the Rakovec Group along the northern and eastern boundary of the early Palaeozoic of the Gemeric Unit in Slovakia, metamorphosed under the high-pressure type of greenschist facies (Faryad and Bernhardt, 1996). Similar compositions are reported for retrogressive amphiboles in eclogites in the Aktyuz area, northern Kyrgyz Tian Shan, Kyrgyzstan (Takasu and Orozbaev, 2009). Potassic-ferro-taramite from a metamorphosed monzonite, Sierra de los Filabres, Andalusia, Spain, was described by Oberti et al. (2008). Chemical analyses corresponding to potassic-ferro-ferri-taramite have been reported for amphiboles rimming arfvedsonite in ilvaite-bearing endoskarn of heterogeneous nepheline syenitic marginal pegmatites in Ilímaussaq, South Greenland (Graser and Markl, 2008).

Regarding magnesian compositions, the "alumino-magnesiotaramite" from a kyanite–eclogite pod, near Selje, Vestlandet, Norway, of Oberti et al. (2007a) corresponds to the present root-name amphibole taramite. Taramite has also been reported from the ultrahigh-pressure metamorphic belt of the Dabie Mountains (Wang et al., 2000) as well as in the Nybø eclogite pod (Norway), formed probably at 0.9–1.3 GPa and 650–720 °C (Ungaretti et al., 1983), and in metabasites at Cóbdar in Sierra de los Filabres, Andalusia, Spain (Puga et al., 2002), formed at 550 °C and 0.8 GPa. Chemical analyses corresponding to potassic-ferri-taramite have been reported in intergranular spaces of an orthopyroxenite xenolith from the Udachnaya-East kimberlite pipe, Daldyn kimberlite field, Siberian platform (Rezvukhin et al., 2020), and interpreted as metasomatic, similar to conditions in the Ilmenogorsky miaskite complex in the South Urals, Russia (Makagonov et al., 2018).

The present paper is the full scientific characterization of the $^{C}Fe^{3+}$ analogue of taramite. Its name, ferri-taramite, is thus dictated by the amphibole nomenclature in force (Hawthorne et al., 2012). The mineral was approved prior to publication by IMA CNMNC (no. 2021-046). The material used here, a skarn sample from the Jakobsberg manganese mine in Sweden, was once examined by Flink (1914), who noted the unusual character of the amphibole and described it as a "strange hornblende". No chemical data were reported for the sample at the time. The holotype material is deposited in the type mineral collection of the Department of Geosciences, Swedish Museum of Natural History, P.O. Box 50007, 10405 Stockholm, Sweden, under collection number GEO-NRM #19221254 (specimen and sections).

2 Occurrence

At the Jakobsberg deposit (59.83° N, 14.11° E; 190 m a.s.l.), 1 km southeast of the Nordmark mine field, Filipstad, Värmland, Sweden, separate hausmannite–braunite and magnetite–hematite ores form distinct bodies adjacent to
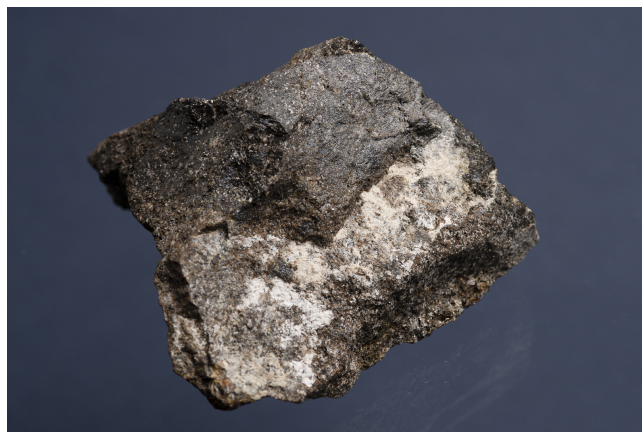

Figure 1. Type specimen, GEO-NRM #19221254, of ferri-taramite (brownish black aggregate on top) with mostly phlogopite (brown) and celsian–baryte (whitish). Field of view 60×100 mm. Torbjörn Lorin photo.

banded skarn–carbonate masses (Magnusson, 1929). It is one of the dolomitic marble-hosted Fe–Mn–(Ba–Pb–As–Sb–Be) Långban-type deposits (Moore, 1970), in the Palaeo-proterozoic Bergslagen ore region. They occur within supracrustal rocks predominated by ∼ 1.9 Ga rhyolitic volcanic–volcaniclastic units, altogether regionally metamorphosed under amphibolite-facies conditions (with a peak at 600–650 °C, 0.3–0.4 GPa) and to some extent also thermally affected by 1.85–1.78 Ga Svecokarelian intrusions (Björck, 1986; Sandström and Holtstam, 1999; Stephens and Jansson, 2020). Genetically, Långban-type deposits constitute metamorphic equivalents of exhalative Mn–Fe deposits in shallow marine environments (Boström et al., 1979; Holtstam and Mansfeld, 2001).

Ferri-taramite occurs as partly poikiloblastic, subhedral crystals up to 5 mm, forming a dense aggregate in a medium-grained skarn (Fig. 1). Associated minerals in the rock are celsian, phlogopite, aegirine-augite, andradite, hancockite, melanotekite, microcline (var. hyalophane), calcite, baryte, prehnite, macedonite and oxyplumboroméite (Fig. 2). Celsian has largely suffered from alteration phenomena, leading to heterogeneous aggregates of various Ba phases with poor crystallinity (Fig. 3). Some portions are similar to cymrite $(BaAl_2Si_2(O,OH)_8 \cdot H_2O)$ in composition, but this mineral could not be confirmed by powder X-ray diffraction. Similar Ba–Pb–Mn–Fe skarn samples from Jakobsberg have been described in the past (Holtstam and Langhof, 1994; Holtstam et al., 2021), but no amphibole was detected, and hence ferri-taramite might be considered relatively rare at the deposit.

3 Physical and optical properties

Ferri-taramite has a short prismatic habitus, along [001]. The colour of the crystals is dark brownish black (greenish yel-
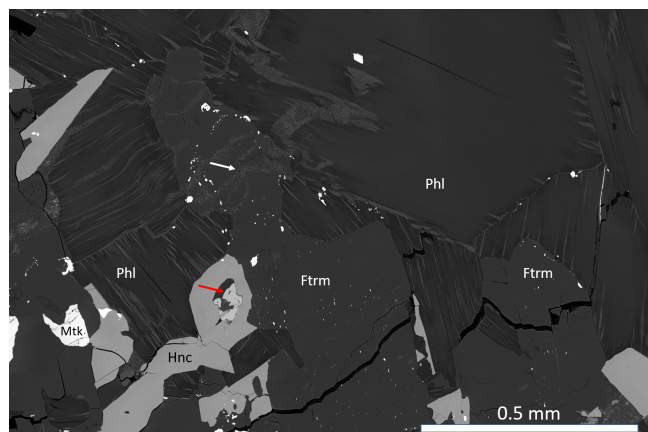
Figure 2. BSE-SEM image of ferri-taramite (Ftrm), with phlogopite (Phl), hancockite (Hnc) and melanotekite (Mtk). The atoll-like hancockite grain contains calcite and baryte (red arrow). The white arrow points to prehnite. White specks in the amphibole crystal are inclusions of macedonite. Sample GEO-NRM #19221254.

low to brown in splinters), with a yellowish grey streak. The lustre is vitreous and semi-transparent, and no fluorescence is observed under UV light. The amphibole is brittle with an uneven to splintery fracture. Cleavage parallel to {110} is good. Hardness (Mohs) is ~ 6. Vickers hardness numbers were obtained on a polished section of ferri-taramite using a micro-hardness tester loaded with a 200 g weight, giving a mean value of 919 (9.0 GPa) for a range of 733–1190 from eight indentations. The density was not measured because of frequent inclusions of heavier minerals (e.g. macedonite); a calculated value is 3.227(5) g cm^{-3} based on the unit-cell volume and atom contents. Ferri-taramite is slightly attracted by a neodymium magnet. It is insoluble in HCl and HNO$_3$.

The optical character is biaxial $(-)$, with $\alpha = 1.670(5)$, $\beta = 1.680(5)$ and $\gamma = 1.685(5)$ in white light and $2V_{\text{meas}} = 70(10)°$ and $2V_{\text{calc}} = 70.2°$. Pleochroism is strong in transmitted light, with X pale yellow, Y dark brown, Z yellowish brown and absorption $Y > Z > X$.

4 Chemical composition

The chemical composition (Table 1) was primarily determined using an FEI Quanta 650 field-emission scanning electron microscope, fitted with an 80 mm^2 X-Max^N Oxford Instruments EDS detector (20 kV, beam size > 1 μm, working distance 10 mm). The beam current was calibrated on Co metal, with the instrument calibrated against metal and mineral standards for each element. The number of point analyses is 10. F and Cl were below detection. Contents of major, minor and other trace elements (Table 2) were also determined with laser-ablation ICP-MS analysis (an NWR 213 nm laser coupled to an Agilent 8800 MS/MS) at the University of Gothenburg, with 16 analysed spots. Element oxide quan-

tification was performed by normalizing to 100 wt %, assuming 2 wt % H$_2$O and the Fe^{2+} / Fe^{3+} ratio from Mössbauer data. We used a multi-standard approach, with measuring calibration factors for each major element from a wide spectrum of known standard materials: NIST SRM 610, ATHO-G, BCR-2G, BHVO-2G, GSC-1G, GSD-1G, Kakanui amphibole, NKT-G, T1-G and TB-1G (all data from the GeoReM database, except for Kakanui amphibole, which is from unpublished electron microprobe data). Consistency of calibration factors is generally better than 4 %, confirming an excellent accuracy when compared with EDS data (Table 1). NIST SRM610 was used as the only primary standard for trace element quantification. The elements P, Cl, Br, Cs, W, Tl, Ta, Bi, Th and U were found to be at or below the level of detection.

The empirical formula of ferri-taramite derived from EDS data and calculated on the basis of 24 (O, OH) is
$^A(\text{Na}_{0.79}\text{K}_{0.16}\text{Pb}_{0.01})_{\Sigma=0.96}$ $^B(\text{Ca}_{1.26}\text{Na}_{0.72}\text{Mn}^{2+}_{0.02})_{\Sigma=2}$
$^C(\text{Mg}_{2.66}\text{Mn}^{2+}_{0.58}\text{Fe}^{2+}_{0.16}\text{Zn}_{0.02}\text{Fe}^{3+}_{1.26}\text{Al}_{0.26}\text{Ti}_{0.06})_{\Sigma=5.00}$
$^T(\text{Al}_{1.86}\text{Si}_{6.14})_{\Sigma=8}\text{O}_{22}$ $^W(\text{OH})_2$. The ideal formula is Na(NaCa)(Mg$_3$Fe$^{3+}_2$)(Si$_6$Al$_2$)O$_{22}$(OH)$_2$, corresponding to the composition SiO$_2$ 41.01 wt %, Al$_2$O$_3$ 11.60 wt %, Fe$_2$O$_3$ 18.16 wt %, MgO 13.75 wt %, CaO 6.38 wt %, Na$_2$O 7.05 wt % and H$_2$O 2.05 wt %, totalling 100.00 wt %.

5 X-ray diffraction data and structure refinement

5.1 Powder data

Powder X-ray diffraction (pXRD) data were collected with a PANalytical X'Pert^3 powder diffractometer equipped with an X'Celerator silicon-strip detector and operated at 40 mA and 45 kV (Cu$K\alpha$ radiation, $\lambda = 1.5406$ Å). The monoclinic, space group $C2/m$ unit-cell parameters refined from the powder data (29 reflections in the 2θ range 9–70°), using least squares with minimization on $Q = 1/d^2$ (Holland and Redfern, 1997), are $a = 9.9019(9)$ Å, $b = 18.0316(16)$ Å, $c = 5.3248(9)$ Å, $\beta = 105.008(8)°$ and $V = 918.31(16)$ Å^3 for $Z = 2$. The complete set of X-ray powder diffraction data is shown in Table 3.

5.2 Crystal structure refinement

A single-crystal X-ray diffraction (SC-XRD) study was done on a $146 \times 213 \times 342$ μm fragment (Fig. 4) using a Rigaku Oxford Diffraction XtaLAB Synergy diffractometer, equipped with a PhotonJet (Mo) X-ray source operating at 50 kV and 1 mA, with monochromatized Mo$K\alpha$ radiation and equipped with a HyPix detector working at 62 mm from the crystal. A combination of ω scans at different values of ϕ, χ and θ positions, with a step scan of 0.5° and exposure time of 2 s per frame, was used to maximize redundancy and data coverage. High-resolution data were collected (up to 0.46 Å).

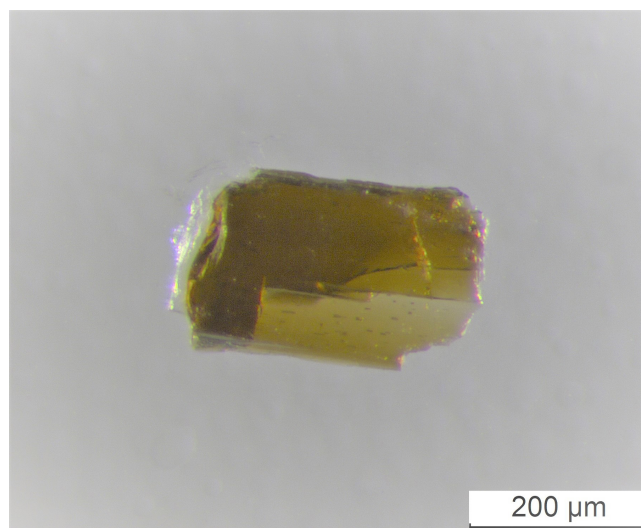**Table 1.** Chemical data (in wt %) for ferri-taramite obtained with EDS and laser-ablation (LA) ICP-MS analyses.

Constituent	EDS, $n = 10$			LA-ICP-MS, $n = 16$		
	Mean	2σ	Range	Mean	2σ	Range
Na_2O	5.26	0.18	5.11–5.42	5.66	0.22	5.50–5.87
MgO	12.06	0.28	11.90–12.40	12.14	0.35	11.90–12.38
Al_2O_3	12.15	1.22	11.61–13.25	11.59	0.59	11.09–12.05
SiO_2	41.43	0.62	40.71–41.73	41.25	0.65	40.55–41.76
K_2O	0.83	0.06	0.77–0.89	0.84	0.05	0.80–0.87
CaO	7.92	0.29	7.53–8.04	8.01	0.27	7.78–8.22
TiO_2	0.50	0.12	0.37–0.58	0.46	0.06	0.39–0.51
MnO	4.81	0.22	4.64–4.98	4.57	0.19	4.35–4.68
Fe_2O_3*	11.30	0.45	11.07–11.73	11.51	0.44	11.11–11.90
FeO*	1.32	0.06	1.28–1.36	1.53	0.06	1.47–1.58
ZnO				0.15	0.01	0.13–0.16
PbO				0.27	0.16	0.22–0.52
BaO				0.05	0.005	0.05–0.06
H_2O_{calc}	2.02			2.02		
Total	99.60			100.00		

* The Fe^{2+} / Fe^{3+} ratio is derived from Mössbauer data. H_2O is calculated on the basis of OH $= 2$ apfu.
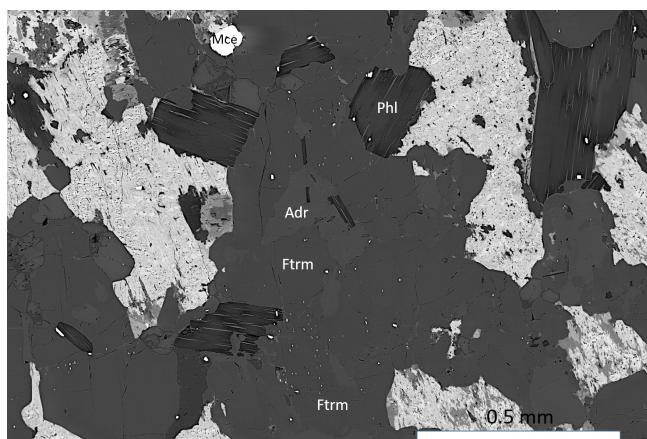
Figure 3. Ferri-taramite with phlogopite, andradite (Adr) and macedonite (Mce). The irregular brighter areas correspond to altered Ba-feldspar. Sample GEO-NRM #19221254.

Figure 4. Crystal fragment of ferri-taramite used for SC-XRD study. Sample GEO-NRM #19221254.

The crystal structure of ferri-taramite was refined starting from the atom coordinates of sample Q99-3 of Oberti et al. (2007a) (named "alumino-magnesiotaramite" in the paper). Scattering curves for fully ionized chemical species were used at sites where chemical substitutions occur; neutral vs. ionized scattering curves were used at the $T(2)$ and anion sites. Scattering at $T(1)$ sites was fixed at the $54 : 46$ $Si^{4+} : Al^{3+}$ ratio as deduced form application of the equation of Oberti et al. (2007b) and in agreement with chemistry. Scattering curves for neutral and fully ionized atoms were taken from International Tables for Crystallography (Wilson, 1992). Splitting of the electron density at site A was observed and added to the model as $A(2)$

and $A(m)$ sites. Full-matrix least-squares refinement on F^2 yielded $R_{obs} = 2.26\%$ (2722 reflections with $I_o > 2\sigma(I)$) and $R_{all} = 2.54\%$ (2983 reflections) using SHELXL (Sheldrick, 2015). See Table 4 for experimental details. Refined atom coordinates, site scattering and equivalent isotropic displacement parameters are reported in Table 5. Selected interatomic distances and bond angles are given in Table 6. Site populations for ferri-taramite have been derived from the unit formula and the results of the structure refinement (Table 7). There is an excellent agreement between the refined values of site scattering (ss, electrons per formula unit) and mean

Table 2. Trace element composition of ferri-taramite ($\mu g\,g^{-1}$).

	Mean(2σ)	Min	Max
As	19(1)	18	21
B	5.5(8)	4.1	7.2
Be	84(5)	75	91
Ce	0.4(1)	0.3	0.4
Co	114(2)	109	117
Cr	294(19)	242	309
Cu	13(7)	6	28
Ga	17(1)	15	18
Ge	1.2(0.3)	0.7	1.9
Hf	0.9(1)	0.6	1.3
In	0.07(1)	0.06	0.09
La	0.08(1)	0.06	0.10
Li	72(4)	66	81
Lu	0.09(1)	0.07	0.11
Mo	1.7(1)	1.5	1.9
Nb	0.04(1)	0.02	0.06
Ni	231(7)	216	244
Rb	1.8(2)	1.5	2.0
Sb	5.1(7)	3.8	6.3
Sc	52(1)	49	54
Sn	0.5(1)	0.3	0.6
Sr	17(1)	15	18
V	6.1(2)	5.7	6.4
Y	1.5(1)	1.2	1.6
Zr	37(2)	34	42

bond lengths (mbl's, Å) and those calculated based on the proposed site populations. A crystallographic information file (CIF) containing observed structure factors has been deposited in the Supplement.

Table 3. X-ray powder diffraction data (d in Å) for ferri-taramite.

I_{obs}	I_{calc}	d_{obs}	d_{calc}	h	k	l
5	32	9.01	9.02	0	2	0
60	**89**	**8.44**	**8.45**	**1**	**1**	**0**
8	23	4.51	4.51	0	4	0
4	2	4.22	4.22	2	2	0
25	**66**	**3.392**	**3.391**	**1**	**3**	**1**
39	**29**	**3.281**	**3.280**	**2**	**4**	**0**
100	**66**	**3.140**	**3.139**	**3**	**1**	**0**
20	30	2.951	2.950	2	2	1
45	**20**	**2.816**	**2.816**	**3**	**3**	**0**
20	34	2.750	2.749	$\bar{3}$	3	1
38	**100**	**2.7104**	**2.7101**	**1**	**5**	**1**
23	53	2.5949	2.5948	0	6	1
17	66	2.5579	2.5580	$\bar{2}$	0	2
8	4	2.3885	2.3886	3	5	0
24	42	2.3473	2.3473	$\bar{3}$	5	1
17	12	2.3398	2.3382	$\bar{4}$	2	1
11	18	2.2969	2.2971	3	1	$\bar{2}$
24	35	2.1654	2.1652	2	6	1
8	15	2.0330	2.0332	4	0	$\bar{2}$
17	18	2.0218	2.0217	3	5	1
14	6	1.9021	1.9022	5	1	0
5	4	1.8655	1.8656	1	9	$\bar{1}$
5	2	1.8224	1.8228	5	3	0
26	13	1.65403	1.65396	4	6	1
13	4	1.63997	1.64011	4	8	0
9	13	1.61565	1.61568	1	11	0
10	13	1.54585	1.54594	6	0	$\bar{2}$
13	10	1.50261	1.50263	0	12	0
33	**31**	**1.44514**	**1.44502**	$\bar{6}$	**6**	**1**
13	**5**	1.36983	1.36989	5	1	2

Note: the seven strongest Bragg reflections are in bold.

6 Spectroscopic data

6.1 Micro-Raman spectroscopy

A Raman spectrum of ferri-taramite (Fig. 5) was collected from a randomly oriented, polished crystal on a LabRAM HR 800 micro-spectrometer, using a 514 nm Ar-ion laser source at < 1 mW power, a Peltier-cooled ($-70\,^{\circ}$C) 1024×256 px CCD detector (Synapse), an Olympus MPlan N $100\times/0.9$ NA objective and a laser spot of ca. 3 µm. A 600 grooves cm^{-1} grating was used, and the resolution is about 1 cm^{-1}. Spectral positions were corrected against the Raman band at 789 cm^{-1} of a SiC-6H crystal measured on {0001}. Instrument control and data acquisition (range 50–4000 cm^{-1}, 10 s exposure time in 20 cycles) were made with the LabSpec 5 software.

The Raman band at ca. 3700 cm^{-1} is related to O–H-stretching vibration modes. Multiple bands in the region 800–1000 cm^{-1} are ascribed to Si–O and ^{T}Al–O symmetric and antisymmetric stretching. The peak at ca. 680 cm^{-1} is assigned to ^{C}Al–O stretching, whereas the one at 669 cm^{-1} corresponds the bending of Si–O–Si bridges (see Waeselmann et al., 2020). The strong peak at 536 cm^{-1} (with a shoulder at ca. 500 cm^{-1}) is tentatively assigned to stretching vibrations of Fe^{3+}–O octahedra and the one at 370 cm^{-1} to Mg–O vibrations.
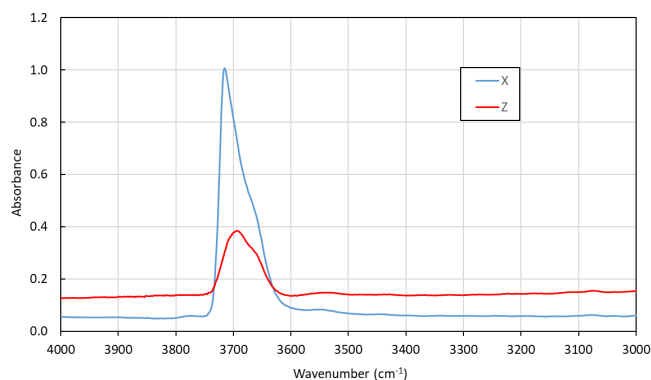
6.2 Fourier-transform infrared (FTIR) spectroscopy

Polarized single-crystal FTIR spectra were collected in the range 2000–10000 cm^{-1} at a spectral resolution of 2 cm^{-1} on a Bruker Vertex 70 spectrometer attached to a Bruker Hyperion 2000 IR microscope. Measurements were done from a 58 µm thick doubly polished single-crystal fragment oriented parallel (010). The spectra (Fig. 6) show a distinct absorption band at 3713 cm^{-1} pronounced in the X direction and caused by O–H-stretching vibrations of the OH dipole at the O(3) position, typical of local ^{A}Na–MgMgMg–SiAl atomic nearest-neighbour and next-nearest-neighbour arrangements of cations around the O(3) atom

Table 4. Crystal data and experimental conditions for SC-XRD study of ferri-taramite.

Temperature	298(2) K
Wavelength	0.71073 Å
Crystal system	Monoclinic
Space group	$C2/m$ (no. 12)
Unit-cell dimensions	$a = 9.89596(13)$ Å
	$b = 18.015(2)$ Å
	$\beta = 105.003(13)°$
	$c = 5.32164(7)$ Å
Unit-cell volume	916.38(2) Å^3
Z	2
Absorption coefficient	2.69 mm^{-1}
Absorption correction	Multi-scan
$F(000)$	873
θ range for data collection	2.26 to 40.64°
Index ranges	$-18 \le h \le 18, -32 \le k \le 32, -9 \le l \le 5$
Reflections collected	17 709
Independent reflections	2983 ($R_{\text{int}} = 2.43$)
Completeness to $\theta = 25.24°$	100 %
Refinement method	Full-matrix least squares on F^2
Data/restraints/parameters	2983/1/121
Goodness of fit on F^2	1.049
Final R indices ($I > 2\sigma(I)$)	$R1 = 0.0226, wR2 = 0.0610$
R indices (all data)	$R1 = 0.0254, wR2 = 0.0625$
Largest diff. peak and hole	1.27 and $-0.99\, e^-$ Å^{-3}
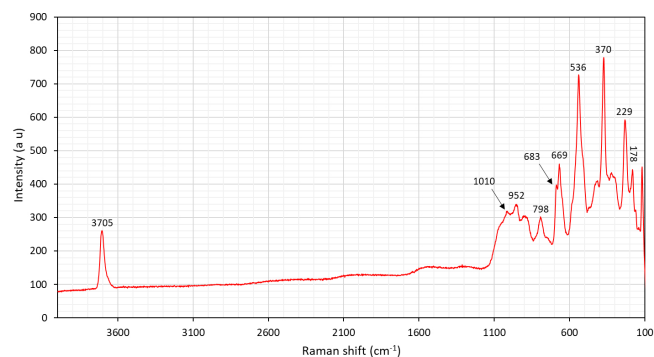
Figure 5. Raman spectrum of ferri-taramite, obtained with a 514 nm laser.

Figure 6. Polarized single-crystal FTIR spectra of ferri-taramite. Sample thickness is 58 µm.

(Hawthorne and Della Ventura, 2007). The interatomic distance from the H atom to the O(7) receptor of 2.67 Å is in good agreement with the main band at 3700 cm^{-1}, based on the known empirical correlations (Libowitsky, 1999). The shoulder band at ca. 3670 cm^{-1} is possibly related to the partial vacancies at the A site. Local ^{A}Na–MnMgMg–SiAl arrangements as a substitution of Mg by Mn^{2+} at $M(1,3)$ is expected to cause a band shift of at least -15 cm^{-1} (see Reece et al., 2002; Hawthorne and Della Ventura, 2007), which may contribute to the observed spectrum.

6.3 Optical absorption spectroscopy

Polarized optical absorption spectra (Fig. 7) were measured on an X–Z crystal section of ferri-taramite (same as used for FTIR). The spectra were recorded in the visible range (350–800 nm) with an AvaSpec-ULS2048x16 spectrometer attached to a Zeiss Axiotron UV microscope. A xenon lamp (75 W) was the light source, and Zeiss Ultrafluar 10× lenses were used as the objective and condenser. The size of the aperture was 30 µm in diameter on the sample. A Glan–Thompson calcite prism served as the polarizer. The spectra show a significant absorption edge towards the

Table 5. Refined atom coordinates and equivalent isotropic displacement parameters.

Atom	Site occ.	x/a	y/b	z/c	U_{eq}
O(1)	O^0 0.23(4) $O^=$ 0.77(4)	0.10680(6)	0.08981(3)	0.21568(11)	0.00961(10)
O(2)	O^0 0.35(4) $O^=$ 0.65(4)	0.12045(6)	0.17356(3)	0.73542(11)	0.00916(10)
O(3)	O^0 0.62(6) $O^=$ 0.38(6)	0.10932(9)	0	0.71219(17)	0.01082(14)
O(4)	O^0 0.49(3) $O^=$ 0.51(3)	0.36651(6)	0.25032(3)	0.79146(11)	0.01046(10)
O(5)	O^0 0.35(4) $O^=$ 0.65(4)	0.35070(6)	0.13886(4)	0.10716(11)	0.01279(11)
O(6)	O^0 0.38(4) $O^=$ 0.62(4)	0.34315(6)	0.11678(4)	0.60895(12)	0.01264(11)
O(7)	O^0 0.25 $O^=$ 0.75	0.33796(10)	0	0.27754(19)	0.01561(16)
$T(1)$	Si^{4+} 0.54 Al^{3+} 0.45	0.28047(2)	0.08614(2)	0.30215(4)	0.00604(5)
$T(2)$	Si^0 0.41(2) Si^{4+} 0.59(2)	0.29088(2)	0.17277(2)	0.81262(4)	0.00648(5)
$M(1)$	Mn^{2+} 0.216(3) Mg^{2+} 0.784(3)	0	0.08949(2)	1/2	0.00755(10)
$M(2)$	Fe^{3+} 0.680(2) Mg^{2+} 0.320(2)	0	0.17851(2)	0	0.00750(6)
$M(3)$	Mn^{2+} 0.270(3) Mg^{2+} 0.730(3)	0	0	0	0.00689(12)
$M(4)$	Ca^{2+} 0.601(2) Na^+ 0.399(2)	0	0.28056(2)	1/2	0.00992(10)
$A(m)$	K^+ 0.030(5)	0.048(3)	1/2	0.097(5)	0.042(6)
$A2$	K^+ 0.033(7) Na^+ 0.437(7)	0	0.4809(2)	0	0.0544(17)
H	1	0.194(4)	0	0.769(6)	0.064(10)

UV, most pronounced in the Z direction. A set of absorption bands caused by spin-forbidden electronic d–d transitions are superimposed on the background. Narrow bands located at ca. 24 500 and 23 000 cm^{-1} mark field-independent transitions in Mn^{2+} and Fe^{3+}, respectively. Broader bands at higher wavelengths, ca. 14 000 cm^{-1}, could be related to $Fe^{2+} \rightarrow Fe^{3+}$ or $Fe^{2+} \rightarrow Ti^{4+}$ charge transfer between neighbouring amphibole octahedra (Burns, 1993).

6.4 Mössbauer spectroscopy

An ^{57}Fe transmission Mössbauer spectrum (Fig. 8) was obtained from a 20 mg powder absorber using ^{57}Co γ radiation and a constant-acceleration spectrometer (WissEl). Two-mirror image spectra (± 4.28 mm s^{-1}) were collected at 54.7° "magic angle" geometry to avoid texture effects, during 70 h over 1024 channels, and calibrated against a 25 μm thick α-iron foil. The baseline of the resulting folded spectrum halted at 6.94×10^6 counts. The MossA software (Prescher et al., 2012) was employed for spectrum analysis, under the assumption of Lorentzian line shapes and a "thin" absorber. A pair of doublets is dominant, with a centroid shift (CS) of 0.388(5) mm s^{-1} and quadrupole splitting (QS) of 0.53(2) and 0.79(2) mm s^{-1}, indicative of Fe^{3+} at an octahedrally coordinated cation site ($M(2)$) with varying nearest-neighbour cation arrangements. A small contri-

Table 6. Selected interatomic distances (Å) and angles (°) in ferri-taramite.

$T(1)$–$O(1)$	1.6614(6)	$T(2)$–$O(2)$	1.6293(6)
$T(1)$–$O(5)$	1.6838(6)	$T(2)$–$O(4)$	1.6025(6)
$T(1)$–$O(6)$	1.6825(6)	$T(2)$–$O(5)$	1.6432(6)
$T(1)$–$O(7)$	1.6695(4)	$T(2)$–$O(6)$	1.6584(6)
$\langle T(1)$–$O\rangle$	1.674	$\langle T(2)$–$O\rangle$	1.633
$M(1)$–$O(1)$ ×2	2.0577(6)	$M(2)$–$O(1)$ ×2	2.0880(6)
$M(1)$–$O(2)$ ×2	2.1238(6)	$M(2)$–$O(2)$ ×2	2.0689(6)
$M(1)$–$O(3)$ ×2	2.1005(6)	$M(2)$–$O(4)$ ×2	1.9651(6)
$\langle M(1)$–$O\rangle$	2.094	$\langle M(2)$–$O\rangle$	2.040
$M(3)$–$O(1)$ ×4	2.0133(6)	$M(4)$–$O(2)$ ×2	2.4359(6)
$M(3)$–$O(3)$ ×2	2.0914(6)	$M(4)$–$O(4)$ ×2	2.3497(6)
$\langle M(3)$–$O\rangle$	2.099	$M(4)$–$O(5)$ ×2	2.6574(7)
		$M(4)$–$O(6)$ ×2	2.5752(7)
		$\langle M(4)$–$O\rangle$	2.505
$A(2)$–$O(5)$ ×2	2.757(3)	$A(2)$–$A(2)$	0.689(8)
$A(2)$–$O(6)$ ×2	2.857(3)	$A(2)$–$A(m)$	0.69(3)
$A(2)$–$O(7)$ ×2	2.4396(10)	$A(m)$–$A(m)$	1.20(6)
$\langle A(2)$–$O\rangle$	2.694		
$A(m)$–$O(5)$ ×2	3.180(17)	$O(3)$–H	0.81(4)
$A(m)$–$O(5)$ ×2	3.002(12)		
$A(m)$–$O(6)$ ×2	2.677(18)	$T(1)$–$O(5)$–$T(2)$	133.90(4)
$A(m)$–$O(7)$	2.50(2)	$T(1)$–$O(6)$–$T(2)$	137.29(4)
$A(m)$–$O(7)$	2.53(2)	$T(1)$–$O(7)$–$T(1)$	136.70(6)
$\langle A(m)$–$O\rangle$	2.845		
		$O(5)$–$O(6)$–$O(5)$	162.72(8)
		$O(6)$–$O(7)$–$O(6)$	100.46(8)

Figure 7. Polarized single-crystal optical spectra of ferri-taramite.

Figure 8. Transmission ^{57}Fe Mössbauer spectrum of ferri-taramite. Subspectra no. 1 (59 %) and no. 2 (29 %) correspond to ^{M2}Fe^{3+}, and no. 3 corresponds to ^{M1,M3}Fe^{2+} (12 %).
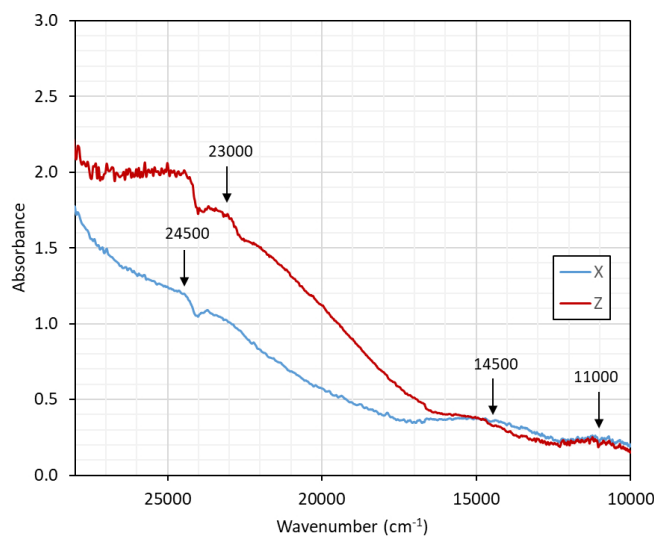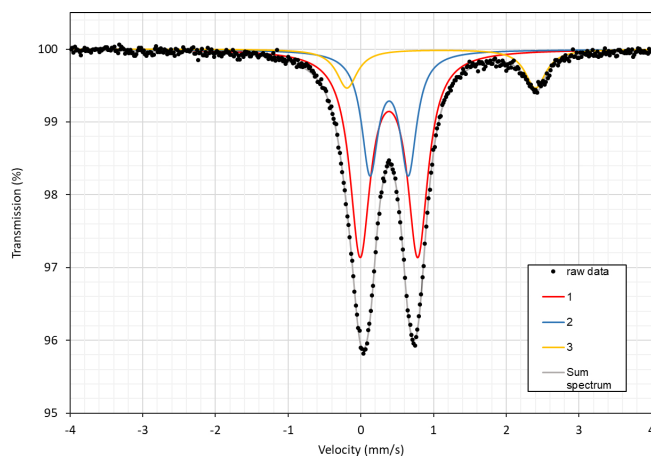
bution, ca. 12 % of total absorption as determined from area ratios (with identical recoil-free fractions assumed for all Fe sites), emanating from another doublet at CS = 1.11(1) and QS = 2.60(2) mm s^{-1} is attributed to Fe^{2+} in octahedral coordination ($M(1)$ and $M(3)$ sites). Line widths (FWHM) were in the range 0.28(2)–0.35(2) mm s^{-1}, with a χ^2 value of 0.9 for the fitting result.

7   Discussion

7.1   Crystal structure and chemistry

Site populations (Hawthorne et al., 1995) were calculated based on present knowledge of amphibole crystal chemistry. The results are reported in Table 7. Here we describe the different cation and anion groups.

   T *sites*. The observed $\langle T(1)$–$O\rangle$ distance is in perfect agreement with the calculated values using the equations of Oberti et al. (2007b; see Tables 6 and 7) and the chemical analyses. Therefore, the 54 : 46 Si^{4+} : Al^{3+} ratio was fixed at

the last stages of refinement. The limited presence of Al in the $T(2)$ sites assumed in Table 7 (2 % per site) is observed in high-temperature high-^{T}Al amphiboles, in agreement with peak conditions for its crystallization (see paragenesis section).

   C-*group cation sites*. On the basis of the observed mean bond lengths, for ^{C}Mn^{2+} the following (strong) site preference is inferred: $M(1) = M(3) \gg M(2)$. This is similar to what is expected for ^{C}Fe^{2+} according to present knowledge of amphibole crystal chemistry (see the review in Oberti et al., 2007b), and it is related to the structural relaxation of $M(1)$ and $M(3)$ sites as a consequence of the size reduction of the adjacent $M(2)$ sites. As in other taramitic amphibole samples (Oberti et al., 2007a), the observed mean octahedral distances are larger than the calculated values, although in

Table 7. Site occupancies for ferri-taramite with site scattering (ss) and mean bond lengths (mbl's).

| Site	Site population (apfu)	ss (epfu)		mbl (Å)	
		Refined	Calculated	Refined	Calculated
$T(1)$	$2.14\,Si^{4+} + 1.86\,Al^{3+}$			1.675	1.675*
$T(2)$	$3.92\,Si^{4+} + 0.08\,Al^{3+}$			1.633	1.633
$M(1)$	$1.56\,Mg^{2+} + 0.33\,Mn^{2+} + 0.11\,Fe^{2+}$	29.62	29.83	2.094	2.096
$M(2)$	$1.26\,Fe^{3+} + 0.37\,Mg^{2+} + 0.26\,Al + 0.06\,Ti^{4+} + 0.04\,Mn^{2+} + 0.01\,Fe^{2+}$	43.04	43.16	2.040	2.025
$M(3)$	$0.73\,Mg^{2+} + 0.21\,Mn^{2+} + 0.04\,Fe^{2+} + 0.02\,Zn^{2+}$	15.52	15.65	2.099	2.101
$\Sigma\,C$ cations		88.18	88.64		
B cations	$1.26\,Ca^{2+} + 0.72\,Na + 0.02\,Mn^{2+}$	32.81	33.62		
A cations	$0.79\,Na^{+} + 0.16\,K^{+} + 0.01\,Pb^{2+}$	12.02	12.55		
W anions	$2\,OH^{-}$				

* Using the equation of Oberti et al. (2007b).

this case the differences are within 0.002 Å, probably related to the fact that the presence of Fe^{3+} in $M(2)$ does not allow for a strong relaxation of this site. In fact, the observed mean octahedral bond length for $M(2)$ site is larger than the calculated value (Table 7). At any rate, the very good agreement between observed and calculated site scattering (a remarkable one) is obtained considering some disordering of Mn^{2+} and Fe^{2+} among the C sites, probably due to the relatively high T of crystallization in the amphibolite facies (see the following).

B-*group cation sites.* The $M(4)$ site shows the typical y/b coordinate of a Ca and/or Na populated site. No evident residual electron density has been found around the $M(4)$ sites in agreement with the absence of Mg and negligible Mn^{2+} at the B-group sites, based on the chemical analyses.

A-*group cation sites.* The A cations are preferentially ordered, with K at the $A(m)$ site (0.066 apfu of K) and Na (0.873 apfu of Na and minor 0.06 apfu of K) at the $A(2)$ subsite (0.57 and 10.87 epfu, respectively). Both K and Na contents agree reasonably well with the chemical analysis ($Na_{0.79}K_{0.16}Pb_{0.01}$). The main preference for $A(2)$ (see Figs. 9 and 1 of Oberti et al., 2007a, for comparison) is also observed in ferro-taramite and taramite related to the preferred local arrangement $^{M(4)}$Ca–$^{O(3)}$OH–$^{A(2)}$Na, although higher occupancy of $A(m)$ sites would be expected due to the local arrangement $^{M(4)}$Na–$^{O(3)}$OH–$^{A(m)}$Na. This might be due to the absence of $^{O(3)}$F, responsible for ordering at the $A(m)$ sites observed in fluoro-taramite (Oberti et al., 2007a). When the A site is dominantly populated by K, like in potassic-ferro-taramite, strong ordering of K at the $A(m)$ site is also observed even in the absence of F at O(3) (Oberti et al., 2008).

W *anion sites.* Despite a relatively high Ti content of 0.06 apfu, there is no indication of deprotonation and existence of an oxy-component ($^{W}O^{2-}$) in ferri-taramite, which is consistent with the metamorphic origin of ferri-taramite (see Oberti et al., 2015b).
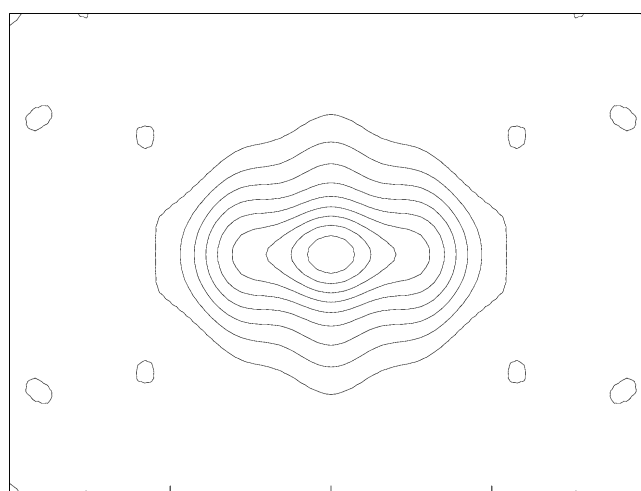
Figure 9. A section of the F_{o} map calculated parallel to $(\bar{2}01)$ and centred at 0, 1/2, 0 for ferri-taramite, showing the distribution of the electron density within the A cavity. The b axis is horizontal, and contours are drawn with steps of $1\,e\,Å^{-1}$ starting from 1.

7.2 Trace elements

Ferri-taramite from Jakobsberg is low in most trace elements. Increased levels, compared to the continental-crust average, are however seen for Be, As, Sb and Pb, which can be considered a Långban-type signature reflecting the general enrichment of these elements in the skarn (Holtstam and Mansfeld, 2001). There is also a significant concentration of the transition elements Sc, Cr, Co, Ni and Zn. Global comparisons are hampered by the fact that comprehensive trace element data for amphiboles of an unmistakable non-igneous origin are very rare. Cr and Co concentrations are slightly enriched compared to an amphibolite-grade hornblende from the Njurundukan mafic complex, Baikal, Russia (samples 487, 499, 23 and 54/3 in Skublov and Drugova, 2003). Concentrations for other elements available for comparison, such as

Y, La, Ce, Lu, Hf and Ta, are significantly lower in ferri-taramite. This effect can possibly be explained (in the case of REE) by the coeval crystallization of ferri-taramite with hancockite that has an epidote-type structure. Amphibole in a magmatic-influenced skarn can show considerably higher Sr, Rb, Sn and Ta contents but is generally lower in the period-4 transition elements (e.g. Žáček, 2007) than seen for ferri-taramite. The partitioning behaviour of trace elements among major skarn-forming minerals (where there is no melt phase present) is, however, essentially unexplored.

7.3 Paragenesis

Amphibole in Mn skarn assemblages is common in Långban-type deposits and mostly occurs as sodic–calcic, aluminium-poor members, $\Sigma T \sim 8\mathrm{Si}$, of the richterite–potassic–richterite series (Sundius, 1945; Holtstam et al., 2019a). Although hastingsitic and pargasitic members ($\Sigma T \sim 6\mathrm{Si} + 2\mathrm{Al}$) are reported as well (e.g. Christy and Gatedal, 2005; Hålenius and Bosi, 2012), they are less frequently encountered. Specimens are Mn-bearing to various extents, with Mn^{2+} acting as both B- and C-group cations. In the case of rare hjalmarite, $^{B}\mathrm{Mn} > {}^{B}\mathrm{Ca}$ (Holtstam et al., 2019b).

The rock with ferri-taramite formed during regional metamorphism as is the case for the above-mentioned amphiboles in general. In a possible scenario, precipitates of Fe–Mn (hydroxy-)oxides, Ca–Mg–Ba–Pb carbonates and siliceous material of hydrothermal origin were mixed with aluminous detritus and reacted to eventually form a skarn assemblage of amphibole, mica, feldspar, clinopyroxene and Pb silicates. The alkali metals have probably originally been derived from metasomatic alteration of the felsic volcanic units (see Magnusson, 1930). Conditions for ferri-taramite formation, close to peak-metamorphism (at circa 650 °C and 0.4 GPa), demonstrably included silica undersaturation, a slightly peralkaline character and relatively high oxygen fugacities of the system. Obviously, hydrous alteration has affected the Jakobsberg skarn at some point, but the amphibole shows little sign of breakdown (limited prehnite formation).

Katophorite, also a rare species (Oberti et al., 2015a), can be considered an intermediate amphibole composition between richterite and taramite, related by the exchange $^{C}\mathrm{Mg}_5 + {}^{T}\mathrm{Si}_8 \rightarrow {}^{C}(\mathrm{Mg}_4\mathrm{Al}) + {}^{T}(\mathrm{AlSi}_7) \rightarrow {}^{C}(\mathrm{Mg}_3\mathrm{Al}_2) + {}^{T}(\mathrm{Al}_2\mathrm{Si}_6)$ (or with $^{C}\mathrm{Fe}^{3+}$ instead of $^{C}\mathrm{Al}$, for the "ferri-" members). It is however not known from the Långban-type deposits. Although the proper bulk compositions could likely be achieved in the rocks present, katophoritic amphiboles seem to belong to a high-pressure domain (Harlow and Sorensen, 2005; Pirard and Hermann, 2015; Oberti et al., 2015a). Ferri-taramite must be a rare composition since we have found very few verified analyses elsewhere in the literature (see Schumacher, 2007). In addition, the present specimen is the first example of a taramitic amphibole from a skarn, not associated with

rock types of magmatic origin. The closest composition to ferri-taramite has been reported from eclogites in the Aktyuz area, northern Kyrgyz Tian Shan, Kyrgyzstan (Takasu and Orozbaev, 2009), but without a direct $\mathrm{Fe}^{2+} / \mathrm{Fe}^{3+}$ determination and with very similar Fe^{3+} and Al^{VI} content, it is difficult to discern if these samples are ferri-taramite or taramite. In the Ilmenogorsky complex in the South Urals, analysis no. 49 of Nikandrov et al. (2000) can be also classified as ferri-taramite, although it is richer in Fe^{3+} than our sample from the type locality. Similar compositions are reported by Makagonov et al. (2018) from the same locality, but Ca at the B site of the amphibole is 1.49 apfu, and the amphibole is therefore very close to magnesio-hastingsite in composition.

References

Björck, L.: Beskrivning till berggrundskartan Filipstad NV, Sver. Geol. Undersök., Swedish Geological Survey, series Af, 147, 1–110, 1986.

Boström, K., Rydell, H., and Joensuu, O.: Långban – An exhalative sedimentary deposit?, Econ. Geol., 74, 1002–1011, https://doi.org/10.2113/gsecongeo.74.5.1002, 1979.

Burns, R. G.: Mineralogical applications of crystal field theory (No. 5), Cambridge University Press, 551 pp., https://doi.org/10.1017/CBO9780511524899, 1993.

Christy, A. G. and Gatedal, K.: Extremely Pb-rich rock-forming silicates including a beryllian scapolite and associated minerals in a skarn from Långban, Värmland, Sweden. Mineral. Mag., 69, 995–1018, https://doi.org/10.1180/0026461056960304, 2005.

Compagnoni, R. and Rolfo, F.: Characteristics of UHP pelites, gneisses, and other unusual rocks, Internat. Geol. Rev., 41, 552–570, https://doi.org/10.1080/00206819909465157, 1999.

Faryad, S. W. and Bernhardt, H.-J.: Taramite-bearing metabasites from Rakovec (Gemeric unit, the western Carpathians), Geol. Carpathica, 47, 349–357, 1996.

Flink, G.: Bidrag till Sveriges mineralogi III, Ark. Kem. Mineral. Geol., 5, 1–273, 1914.

Giret, A., Bonin, B., and Leger, J. M.: Amphibole compositional trends in oversaturated and undersaturated alkaline plutonic ring-composition, Can. Mineral., 18, 481–495, 1980.

Graser, G. and Markl, G.: Ca-rich ilvaite–epidote–hydrogarnet endoskarns: a record of late-magmatic fluid influx into the persodic Ilímaussaq Complex, South Greenland, J. Petrol., 49, 239–265, https://doi.org/10.1093/petrology/egm079, 2008.

Hålenius, U. and Bosi, F.: Cation ordering in Pb^{2+}-bearing, Mn^{3+}-rich pargasite from Långban, Sweden. Am. Mineral., 97, 1635–1640, https://doi.org/10.2138/am.2012.4137, 2012.

Harlow, G. E. and Sorensen, S. S.: Jade (nephrite and jadeitite) and serpentinite: metasomatic connections, Inter. Geol. Rev, 47, 113–146, https://doi.org/10.2747/0020-6814.47.2.113, 2008.

Hawthorne, F. C. and Grundy, H. D.: The crystal chemistry of the amphiboles, VII. The crystal structure and site chemistry of potassian ferri-taramite, Can. Mineral., 16, 53–62, 1978.

Hawthorne, F. C. and Della Ventura, G.: Short range order in amphiboles, in: Amphiboles: Crystal chemistry, occurrence and health issues, edited by: Hawthorne, F. C., Oberti, R., Della Ventura, G. and Mottana, A., Rev. Mineral. Geochem., 67, 173–222, 2007.

Hawthorne, F. C., Ungaretti, L., and Oberti, R.: Site populations in minerals: Terminology and presentation of results of crystal-structure refinement, Can. Mineral., 33, 907–911, 1995.

Hawthorne, F. C., Oberti, R., Harlow, G. E., Maresch, W. V., Martin, R. F., Schumacher, J. C., and Welch, M. D.: Nomenclature of the amphibole supergroup, Am. Mineral., 97, 2031–2048, https://doi.org/10.2138/am.2012.4276, 2012.

Holland, T. J. B. and Redfern, S. A. T.: Unit cell refinement from powder diffraction data: the use of regression diagnostics, Mineral. Mag., 61, 65–77, https://doi.org/10.1180/minmag.1997.061.404.07, 1997.

Holtstam, D. and Langhof, J.: Hancockite from Jakobsberg, Filipstad, Sweden: the second world occurrence, Mineral. Mag., 58, 172–174, https://doi.org/10.1180/minmag.1994.058.390.18, 1994.

Holtstam, D. and Mansfeld, J.: Origin of a carbonate-hosted Fe-Mn-(Ba-As-Pb-Sb-W) deposit of Långban-type in Central Sweden, Mineral. Dep., 36, 641–657, 2001.

Holtstam, D., Cámara, F., Skogby, H., Karlsson, A., and Langhof, J.: Description and recognition of potassic-richterite, an amphibole supergroup mineral from the Pajsberg ore field, Värmland, Sweden, Mineral. Petrol., 113, 7–16, https://doi.org/10.1007/s00710-018-0623-6, 2019a.

Holtstam, D., Cámara, F., Skogby, H., and Karlsson, A.: Hjalmarite, a new Na–Mn member of the amphibole supergroup, from Mn skarn in the Långban deposit, Värmland, Sweden, Eur. J. Mineral., 31, 565–574, https://doi.org/10.1127/ejm/2019/0031-2822, 2019b.

Holtstam, D., Cámara, F., and Karlsson, A.: Instalment of the margarosanite group, and data on walstromite–margarosanite solid solutions from the Jakobsberg Mn–Fe deposit, Värmland, Sweden, Mineral. Mag., 85, 224–232, https://doi.org/10.1180/mgm.2021.15, 2021.

Libowitzky, E.: Correlation of OH stretching frequencies and OH…O hydrogen bond lengths in minerals, Monatsh. Chem., 130, 1047–1059, https://doi.org/10.1007/BF03354882, 1999.

Magnusson, N. H.: Nordmarks malmtrakt: geologisk beskrivning, Sver. Geol. Undersök, Swedish Geological Survey, series Ca, 13, 1–98, 1929.

Magnusson, N. H.: Långbans malmtrakt, Sver. Geol. Undersök, Swedish Geological Survey, series Ca, 23, 1–111, 1930.

Makagonov, E. P., Kotlyarov, V. A., and Korinevsky, E. V.: Amphiboles of alkaline rocks of the Ilmenogorsky Complex and country metamorphic rocks, South Urals, Mineralogiya, 4, 8–26, 2018 (in Russian).

Moore, P. B.: Mineralogy & chemistry of Långban-type deposits in Bergslagen, Sweden, Mineral. Record, 1, 154–172, 1970.

Morozewicz, J.: Über einige Eisenalkali-amphibole, Tscher. Miner. Petrog., 38, 210–222, https://doi.org/10.1007/BF02993932, 1925.

Nikandrov, S. N., Kobyashev, Y. S., and Valizer, P. M.: Amphiboles of the Ilmenogorsky complex. IGZ UB RAS (Ilmensky State Reserve, Ural branch of the Russian Academy of Sciences), Miass, Russia, 120 pp., 2000 (in Russian).

Oberti, R., Boiocchi, M., Smith, D. C., and Medenbach, O: Aluminotaramite, alumino-magnesiotaramite, and fluoro-alumino-magnesiotaramite: Mineral data and crystal chemistry, Am. Mineral., 92, 1428–1435, https://doi.org/10.2138/am.2007.2529, 2007a.

Oberti, R., Hawthorne, F. C., Cannillo, E., and Cámara, F.: Long-range order in amphiboles, in: Amphiboles: Crystal chemistry, occurrence and health issues, edited by: Hawthorne, F. C., Oberti, R., Della Ventura, G., and Mottana, A., Rev. Mineral. Geochem., 67, 125–172, https://doi.org/10.2138/rmg.2007.67.4, 2007b.

Oberti, R., Boiocchi, M., Smith, D. C., Medenbach, O., and Helmers, H.: Potassic-aluminotaramite from Sierra de los Filabres, Spain. Eur. J. Mineral., 20, 1005–1010, https://doi.org/10.1127/0935-1221/2008/0020-1837, 2008.

Oberti, R., Boiocchi, M., Hawthorne, F. C., Ball, N. A., and Harlow, G. E.: Katophorite from the Jade Mine Tract, Myanmar: mineral description of a rare (grandfathered) endmember of the amphibole supergroup, Mineral. Mag., 79, 355–363, https://doi.org/10.1180/minmag.2015.079.2.13, 2015a.

Oberti, R., Boiocchi, M., Hawthorne, F. C., Cámara, F., Ciriotti, M. E., and Berge, S. A.: Ti-rich fluoro-richterite from Kariåsen (Norway): the oxo-component and the use of Ti^{4+} as a proxy, Can. Mineral., 53, 285–294, https://doi.org/10.3749/canmin.1400086, 2015b.

Pirard, C. and Hermann, J.: Experimentally determined stability of alkali amphibole in metasomatised dunite at sub-arc pressures, Contrib. Mineral. Petrol., 169, 1–26, https://doi.org/10.1007/s00410-014-1095-2, 2015.

Prescher, C., McCammon, C., and Dubrovinsky, L.: MossA: a program for analyzing energy-domain Mössbauer spectra from conventional and synchrotron sources, J. Appl. Cryst., 45, 329–331, https://doi.org/10.1107/S0021889812004979, 2012.

Puga, E., Ruiz-Cruz, M. D., and Diaz de Federico, A.: Polymetamorphic amphibole veins in metabasalts from the betic ophiolitic association at Cóbdar, southeastern Spain: relics of ocean-floor metamorphism preserved through the alpine orogeny, Can. Mineral., 40, 67–83, https://doi.org/10.2113/gscanmin.40.1.67, 2002.

Reece, J. J., Redfern, S. A. T., Welch, M. D., Henderson, M. B., and McCammon, C. A.: Temperature-dependent Fe^{2+}–Mn^{2+} order–disorder behaviour in amphiboles, Phys. Chem. Minerals, 29, 562–570, https://doi.org/10.1007 s^{-1}00269-002-0267-1, 2002.

Rezvukhin, D. I., Alifirova, T. A., Golovin, A. V., and Korsakov, A. V.: A plethora of epigenetic minerals reveals a multistage metasomatic overprint of a mantle orthopyroxenite from the Udachnaya Kimberlite, Minerals, 10, 264, https://doi.org/10.3390/min10030264, 2020.

Sandström, F. and Holtstam, D.: Geology of the Långban deposit, in: Långban: the mines, their minerals, geology and explorers, edited by: Holtstam, D. and Langhof, J., Naturhistoriska riksmuseet and Raster Förlag, Stockholm, ISBN 91 87214 881, 1999.

Schumacher, J. C.: Metamorphic amphiboles: composition and coexistence, Rev. Mineral. Geochem., 67, 359–416, https://doi.org/10.2138/rmg.2007.67.10, 2007.

Sheldrick, G. M.: Crystal structure refinement with SHELXL, Acta Cryst., C71, 3–8, https://doi.org/10.1107/S2053229614024218, 2015.

Skublov, S. and Drugova, G.: Patterns of trace-element distribution in calcic amphiboles as a function of metamorphic grade, Can. Mineral., 41, 383–392, https://doi.org/10.2113/gscanmin.41.2.383, 2003.

Stephens, M. B. and Jansson, N. F.: Paleoproterozoic (1.9–1.8 Ga) syn-orogenic magmatism, sedimentation and mineralization in the Bergslagen lithotectonic unit, Svecokarelian orogen, Geol. Soc. Mem., 50, 155–206, https://doi.org/10.1144/M50-2017-40, 2020.

Sundius, N.: The position of richterite in the amphibole group, Geol. Fören. Stock. För., 67, 266–270, https://doi.org/10.1080/11035894509446100, 1945.

Takasu, A. and Orozbaev, R.: Variety of chemical compositions of amphiboles from eclogites in the Aktyuz area, northern Kyrgyz Tien-Shan, Geoscience Report Shimane Univ., Shimane University, 28, 51–63, 2009.

Ungaretti, L., Smith, D. C., and Rossi, G.: Crystal-chemistry by X-ray structure refinement and electron microprobe analysis of a series of sodic-calcic to alkali-amphiboles from the Nybö eclogite pod, Norway, Bull. Minéral., 104, 400–412, 1983.

Waeselmann, N., Schlüter, J., Malcherek, T., Della Ventura, G., Oberti, R., and Mihailova, B.: Nondestructive determination of the amphibole crystal-chemical formulae by Raman spectroscopy: One step closer, J. Raman Spectrosc., 51, 1530–1548, https://doi.org/10.1002/jrs.5626, 2020.

Wang, R., Xu, S., and Xu, S.: First occurrence of preiswerkite in the Dabie UHP metamorphic belt, Chinese Sci. Bull., 45, 748–750, https://doi.org/10.1007/BF02886183, 2000.

Wilson, A. J. C.: International Tables for Crystallography, Volume C: Mathematical, physical and chemical tables, Kluwer Academic, Dordrecht, Netherlands, 883 pp., ISBN 0-792-3-16-38X, 1992.

Žáček, V.: Potassian hastingsite and potassichastingsite from garnet hedenbergite skarn at Vlastejovice, Czech Republic, Neues Jb. Miner. Abh., 2007, 161–168, https://doi.org/10.1127/0077-7757/2007/0089, 2007.

Zhang, R. Y. and Liou, J. G.: Coesite-bearing eclogite in Henan Province, central China: detailed petrography, glaucophane stability and PT-path, Eur. J. Mineral., 9, 217–234, https://doi.org/10.1127/ejm/6/2/0217, 1994.